Distribution Agreement

In presenting this thesis as a partial fulfillment of the requirements for a degree from Emory University, I hereby grant to Emory University and its agents the non-exclusive license to archive, make accessible, and display my thesis in whole or in part in all forms of media, now or hereafter now, including display on the World Wide Web. I understand that I may select some access restrictions as part of the online submission of this thesis. I retain all ownership rights to the copyright of the thesis. I also retain the right to use in future works (such as articles or books) all or part of this thesis.

Yilin Zhang April 12, 2016

Control of Amyloid Beta Peptide Self-Assembly

by

Yilin Zhang

Dr. David G. Lynn
Adviser

Department of Chemistry

Dr. David G. Lynn

Adviser

Dr. Roger Deal

Committee Member

Dr. Jose Soria

Committee Member

2016

Control of Amyloid Beta Peptide Self-Assembly

By

Yilin Zhang

Dr. David G. Lynn

Adviser

An abstract of
a thesis submitted to the Faculty of Emory College of Arts and Sciences
of Emory University in partial fulfillment
of the requirements of the degree of
Bachelor of Sciences with Honors

Department of Chemistry

2016

Abstract

Control of Amyloid Beta Peptide Self-Assembly

By Yilin Zhang

The self-assembly of amyloid beta peptide forms plaque, some of which cause Alzheimer's disease. Assembly depends on the tissue environment. The Dutch mutant model, Aβ(16-22) E22Q, reveals clear progressive stages of assembly, from particle formation to para-crystalline mutation, that can now be used to control the various stages of assembly. Changes in the dielectric of the media, the shear forces on the assemblies, and site-specific substitutions now provide insight into strand orientation, strand registry, fiber twisting and bundling, and ribbon helicity. An initial structural code is now emerging where the rate of progression through various intermediates and the final architecture of the assembly can be controlled to construct well-defined mesoscale materials.

Control of Amyloid Beta Peptide Self-Assembly

By

Yilin Zhang

Dr. David G. Lynn

Adviser

A thesis submitted to the Faculty of Emory College of Arts and Sciences
of Emory University in partial fulfillment
of the requirements of the degree of
Bachelor of Sciences with Honors

Department of Chemistry

2016

Acknowledgements

First and foremost, I would like to thank Dr. David Lynn for all the extraordinary supports and encouragements during my time in lab. He kindly read my thesis and offered invaluable detailed advices on grammar, organization, and the theme of the thesis.

Second, I would like to thank Dr. Roger Deal and Dr. Jose Soria for their times and commitments to serve as my committee members, and for all the suggestions that greatly improved this thesis.

Finally, I would like to thank Chen and Jill for teaching me all the lab techniques and helping me with all the lab projects.

Table of Contents

List of Figures

Control of Amyloid Beta Peptide Self-Assembly

Yilin Zhang

Department of Chemistry, Emory University, Atlanta, GA, 30322

yzha368@emory.edu

ABSTRACT: The self-assembly of amyloid beta peptide forms plaque, some of which cause Alzheimer's disease. Assembly depends on the tissue environment. The Dutch mutant model, Aβ(16-22) E22Q, reveals clear progressive stages of assembly, from particle formation to para-crystalline mutation, that can now be used to control the various stages of assembly. Changes in the dielectric of the media, the shear forces on the assemblies, and site-specific substitutions now provide insight into strand orientation, strand registry, fiber twisting and bundling, and ribbon helicity. An initial structural code is now emerging where the rate of progression through various intermediates and the final architecture of the assembly can be controlled to construct well-defined mesoscale materials.

INTRODUCTION

The self-assembly of peptides into cross-β sheet forms, commonly known as amyloids, underlies the development of many human diseases, including the most common neurodegenerative disease, Alzheimer's disease (AD).[1] The pathology of AD is associated with amyloid beta (Aβ) peptides[2], which are cleaved from a functional transmembrane protein known as the amyloid precursor protein (AβPP)[3]. The abnormal processing and deposition of Aβ forms extracellular plaques which contribute to dementia.[3] The observations arguing that AD is a progressive disease[2] where the presence of plaque is necessary but not sufficient to cause AD[3] implicate other contributing factors. The evolutionary features of the progressive infection suggest that the self-assembly of Aβ could access many different para-crystalline structures that are selected in the tissues depending on different neuronal environments.[4] It then becomes critical that the assembly process be explored and the external cues, from salt, pH, solvent, temperature and mechanical agitation, be defined.[5]

Initial insight into the assembly pathway of Aβ model peptides was purposed by Childer et al.[6] in 2012 using the nucleating core of Aβ peptide: Aβ(16-22) Ac-KLVFFAE-NH_2. Peptide monomers, once solvated, formed particles through a classical phase change. Ordered-structures emerged within these particles that propagated into para-crystalline structures in a separate phase change. The propagation into para-crystalline structures required templates for the addition of free peptides through template-directed replication.

The Dutch mutant of this model peptide, Aβ(16-22) (E22Q), Ac-KLVFFAQ-NH_2, carries a substitution of glutamine for glutamic acid at the C-terminal position. Liang et al.[7] observed that different para-crystalline structures could form during the course of assembly. After the initial particle phase, antiparallel out-of-register ribbons and twisted fibers emerged within the particles. This was argued to arise from the charge repulsions of the N-terminal lysines inside the low dielectric environment of the particles. However, this was the kinetic product of the assembly, as propagation in solution gave rise to the parallel in-register fibers via template-directed mutations. The thermodynamic product, the parallel structure, was stabilized by hydrogen bonds formed between glutamines of the adjacent strands. Once the concentration of the parallel fibers reached a certain threshold, strand breakage would generate more catalytic templates such that the parallel structure propagates auto-catalytically.[7] Therefore, the rate of mutation into parallel structure was dependent on both the amount of free fibril ends as well as free the peptide monomer concentrations.

E22Q then becomes a valuable model peptide not only for testing the assembly pathway but also for evaluating the various structural codes and environmental conditions that could be used to control the Aβ cross-β assemblies. According to the mechanism, particle formation should be sensitive to the dielectric constant of the media, and added salt should lower the critical concentration for the phase transition. Thus, addition of salt is hypothesized to increase the rate of assembly and the size of the particles. Further, as the antiparallel to parallel transition requires free monomers and free fibril ends, mechanical agitations like shaking and stirring the assembly solution should contribute to strand breaking, provide more free ends, and increase the rate of mutation from antiparallel to parallel fibers.

With these insights, it should be possible to predict structural codes. For example, in E22Q the parallel structures replaced antiparallel structures as the Q-Q parallel H-bonded structure overwhelmed the electrostatic cross-strand pair. "Code" is used here in analogy to the A/T and G/C molecular codes that dictate nucleic acid assembly. The final assemblies then should be indicated by the relative strengths of these codes, and should be controllable by appropriate use of these codes. L17Q (Ac-KQVFFAE-NH2) is designed to test the strength of the Q-Q hydrogen bonding interactions at another position in the strand. The L17Q substitution also recovers the glutamic acid at the C-terminus, re-introducing the cross-strand salt bridge. Under pH7, the glu22 carries a negative charge, which should stabilize the salt bridge with lys16 in the antiparallel, in-register strand arrangement. Competition with the Q preference for parallel strands will allow the relative strengths of these associations to be tested in head-to-head comparisons.

IE-IR basis sets were introduced by Smith et al.[8] in 2015 to enable the assignment of the relative concentrations of each accessible para-crystalline structures (unassembled monomers; antiparallel, out-of-register structure; antiparallel, in-register structure, and parallel structure) using ^{13}C enriched amino acids. As the anti-parallel to parallel mutation occurs, the splitting between ^{12}C and ^{13}C peak would decrease, and the intensity ratio ($^{12}C/^{13}C$) would increase.[8] In addition, transmission electron microscopy (TEM) is used to visualize the assembly morphologies, and circular dichroism spectropolarimetry (CD) is used to detect the rate of assembly.

Here E22Q assembly is monitored in the presence of 0mM, 10mM, 25mM and 50mM NaCl to evaluate the dependence of assembly on the dielectric of the media. E22Q assemblies are also either shaken by placing on a shaker, or stirred via a stir bar as a way to explore shear force differences. The insight gained from these experiments is then applied to substitutions at L17Q peptides under both acidic and neutral conditions to evaluate the competition of a salt bridge to the Q-track H-bonds of the glutamine residues.

MATERIALS AND METHODS

1. Peptide synthesis and purification

[1-^{13}C]F19 Aβ(16-22)E22Q and [1-^{13}C]F19 Aβ(16-22)L17Q were synthesized according to previously published methods[7]. In brief, all acetylated N-terminus peptides were synthesized using FMOC protected amino acids by Liberty CEM Microwave Automated Peptide Synthesizer (Matthews, NC, USA). Peptides were cleaved from dried resin by placing into a solution containing 90 vol% TFA, 5 vol% thioanisole, 3 vol% ethane dithiol, and 2 vol% anisole for 4 hours at room temperature, and then were precipitated and washed by pure diethyl ether. Peptide purification was performed by reverse-phase HPLC (Waters Delta 600) using a Waters Atlantis C-18 preparative column (19 x 250 mm). Product mass was confirmed by MALDI-TOF on a Voyager-DETM STR Biospectrometry Workstation using α-cyano-4-hydroxycinnamic acid (CHCA) as the matrix.

2. Fibril assembly

For all 4 samples of the E22Q salt project, 1.79 mg of lyophilized [1-^{13}C]F19E22Q peptides were dissolved in 1,1,1,3,3,3-hexafluoro-2-propanol (HFIP) from Sigma-Aldrich (St. Louis, MO, USA) and were sonicated for 30 min. The peptides were then dried under a stream of dry N_2 gas to form a clear film. Same procedures were done to the 3 samples each of 0.45 mg [1-^{13}C]F19E22Q for the E22Q agitation project, and to the 2 samples each of 0.46 mg [1-^{13}C]F19L17Q for the L17Q project.

For the E22Q salt project, the film was dissolved in 2000 µL of 20% acetonitrile/water with 0.1 vol% TFA (1 mM peptide concentration) and bath sonicated for 10 min. The 2000 µL peptide solution was evenly divided into 4 bottles, 3 of which were added with 5 µL of 1 M NaCl solution, 12.5 µL of 1 M NaCl solution, and 6.25 µL of 4 M NaCl solution, respectively. The 4 samples (0mM salt, 10mM salt, 25mM salt and 50mM salt) were then sonicated for another 10 min and were incubated at room temperature for peptides self-assembly.

All 3 films from the E22Q agitation project were each dissolved in 500 µL of 20% acetonitrile/water with 0.1 vol% TFA (1 mM peptide concentration) and bath sonicated for 20 min. One sample was placed on an orbital shaker from Bellco Glass INC (Vineland, NJ, USA) set at 2 for its assembly at room temperature thereafter. One other sample was stirred on the VMR VMS-C4 magnetic hotplate stirrer (Radnor, PA, USA) setting at level 1 by a stir vane during its assembly in room temperature. The other sample was settled still on the bench at room temperature and was barely moved to minimize agitation.

The pH of 20% acetonitrile/water with 0.1 vol% TFA solvent was roughly at 2. For the L17Q project, some solvent was neutralized to pH7 with the additions of 0.1 M NaOH solution. The two L17Q films were dissolved in 500 µL of either pH2 or pH7 solvents (1 mM peptide concentration), bath sonicated for 20 min, and incubated in room temperature.

3. Sample monitoring

Samples of all the three projects were monitored on a daily basis using FT-IR, TEM, and CD.

Fourier Transform Infrared Spectroscopy (FT-IR). Aliquots (10 µL) of peptide solution were dried as thin films on a Pike GaldiATR (Madison, WI, USA) ATR diamond crystal. FT-IR spectra were acquired using a Jasco FT-IR 4100 (Easton, MD, USA) at room temperature and averaging 500 to 800 scans with 2 cm-1 resolution, using either an MCT or TGS detector, 5mm aperture and a scanning speed of 4mm/sec. Spectra were processed with zero-filling and a cosine apodization function. IR spectra recorded from 1000 cm^{-1} to 3600 cm^{-1}, and were normalized to the peak height of the ^{12}C band (at roughly 1638 cm^{-1}), and for the salt project, were de-convoluted to reveal the relative concentration of each para-crystalline structures using Mathematica and the previously published codes[8].

Transmission Electron Microscopy (TEM). To prepare for a TEM grid, 5 µL of peptide solution were diluted to 100 µL, 10 µL of which was pipetted onto the TEM copper grid with a 200 mesh carbon support (Electron Microscopy Sciences, Hatfield, PA, USA) for 2.5 mins, and excess solution was absorbed away with filter paper. The grid was then stained by 2% methylamine tungstate (Sigma-Aldrich, St. Louis, MO, USA) for 3 mins after which excess solution was wicked away, and the grids were placed in a desiccator to dry under vacuum overnight. TEM grids were visualized by the Hitachi (Tokyo, Japan) H-7500 transmission electron microscope at 75kV.

Circular Dichroism Spectropolarimetry (CD). Aliquots (20 µL) of peptide solution were pipetted onto a pair of QS 0.10 mm quartz cells from Hellma (Müllheim, Germany). CD spectra were recorded on a Jasco J-810 CD spectropolarimeter (Easton, MD, USA). Spectra were recorded from 260 to 190 nm at a scanning rate of 100 nm/min and a resolution of 0.5 nm.

RESULTS AND DISCUSSION

1. E22Q Salt Project

1.1. Oligomerization and nucleation at particle phase

The TEM images of E22Q grown in solvents containing 0mM, 10mM, 25mM, and 50mM of salt at day 1 (taken immediately after peptide salvation) are presented in Figure 1 a-d, and Figure 1e shows a zoom-in view for Figure 1b (the 10mM salt sample).

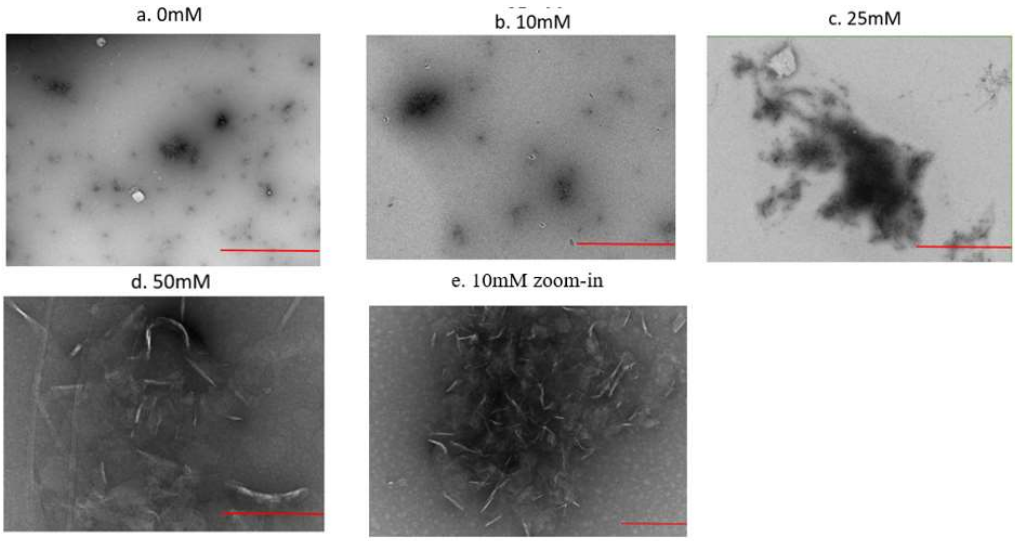

Figure 1. TEM images of samples immediately after E22Q solvated in solvents of a). 0mM, b). 10mM, c). 25mM, and d). 50mM NaCl. e). A zoom-in picture of a particle in 10 mM sample seen in b. For a-d, images are adjusted to the same scale and the scale bar in each image represents 2.0 μm; for e, the scare bar is 200 nm.

Soon after peptide solvation, particles formed as represented by the black spots in the TEM pictures. Nonspecific molecular interactions directed the initial collapse of hydrophobic peptides into disordered aggregates.[9] The size of these particles ranged from oligomer of only a few peptides to micrometer-sized containing thousands of peptides.[4,10] Addition of salt lowered the dielectric constant of the media, and as a result the size of the particles should increase. This trend was clearly indicated in Figure 1, the diameter of the particles increased as salt concentration was raised. Several small particles were observed in the 0 mM sample (Figure 1a), whereas one of the particles formed under 50 mM salt occupied the whole view of Figure 1d.

In addition, as the dehydrated and high dielectric particle grown, specific molecular interactions, including charge-charge repulsions, electrostatic salt bridges and steric interactions, directed the ordering of peptides into cross-β fibers.[7,11] In Figure 1e, the zoom-in picture of one particle found in the 10 mM salt sample, ordered structures seemed to start emerging within the particle. The 25 mM salt sample had more of these ordered structures grew out of the particle (Figure 1c). Further, the emerging para-crystalline structures, the fibers, could clearly be defined in the 50 mM salt sample (Figure 1d). Therefore, the rate of assembly into particles and para-crystalline structures increased as the salt concentration increased.

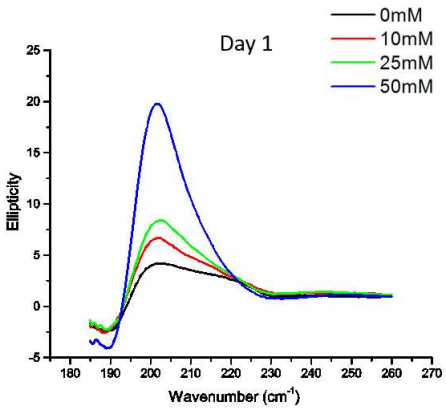

Figure 2. CD spectra of E22Q in solvents of 0mM, 10mM, 25mM, and 50mM salt at day 1.

Figure 2 contains four CD spectra, each from E22Q solvated in solvents with 0mM, 10mM, 25mM, and 50mM salt at day 1. The signature peak indicated the presence of highly ordered structures in the assembly solution. The peak raised as the salt concentration increased (Figure 2), again suggested that the higher the salt concentration, the earlier the emergence of para-crystalline structures within particles.

1.2 Structural mutation during propagation

For all the IR spectra taken from day 1 to day 27 during the course of the assembly under one salt concentration, the amount of splitting between the ^{12}C peak (at roughly 1638 cm^{-1}) and the ^{13}C peak (at roughly 1600 cm^{-1}) versus time was fitted to the Boltzmann function. The fitting curves of assemblies at 0 mM, 10 mM, 25 mM, and 50 mM salt concentration are displayed in Figure 3.

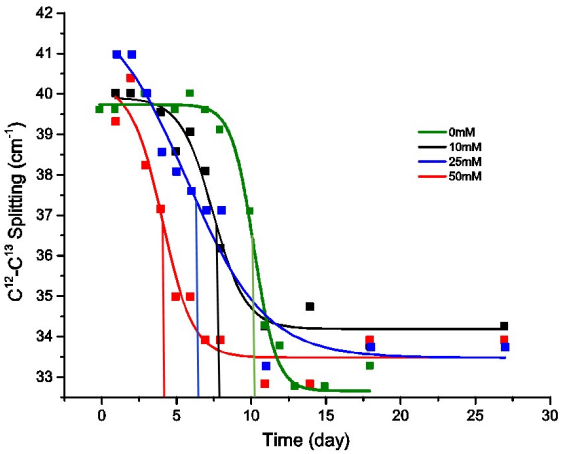

Figure 3. ^{12}C-^{13}C splitting fitting curves for IR spectra of 0mM, 10mM, 25mM and 50mM samples from day 1 to 27. Points represent specific peak splitting distances and are fitted by Boltzmann function. Vertical lines represent the half-time of the structural mutations.

According to the previous study[7] on E22Q self-assembly, as the assembly progressed, template-directed mutations would replace the formerly formed antiparallel, out-of-register fibers with parallel fibers, and only parallel structures could be observed when the assembly completed. The progress of the structural mutation was revealed by the decreasing splitting pattern of between the ^{12}C and ^{13}C peaks in the IR spectra.[8] As shown in Figure 3, the drop down of the splitting occurred earlier as the salt concentration increased. $T_{1/2}$ lines drawn in Figure 3 approximated the time when the structural mutations were happening. The mutations happened at day 4 for the 50 mM salt sample, day 6 for the 25 mM salt sample, day 7 for the 10 mM salt sample, and day 10 for the 0 mM salt sample (Figure 3). These results implied that the higher the salt concentration, the earlier the mutation would occurred, and so the higher the rate of E22Q self-assembly.

The occurrence time of the mutation could also be explained by the screening effect of the salt. Screening of salt weakened the K-K electrostatic repulsions. The antiparallel structures were stabilized, whereas the parallel structures were destabilized by these K-K repulsions. Thus, under high salt concentration, the antiparallel structures were not as favorable while the parallel structures were more favorable compared to assemblies under low salt concentration, and addition of salt speeded up the process of the antiparallel to parallel structural mutations.

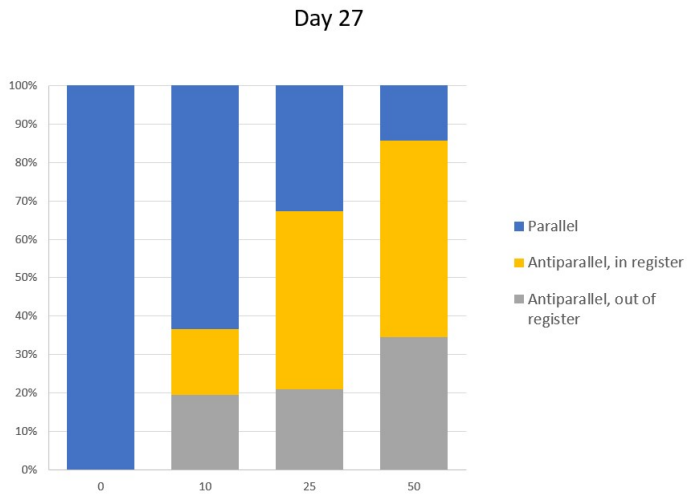

Figure 4. IR spectra deconvolution of 0mM, 10mM, 25mM, and 50mM sample at day 27 to reveal the composition of parallel, antiparallel, in register, and antiparallel, out of register structures in each sample.

The deconvolutions of day 27 IR spectra of the 0mM, 10mM, 25mM, and 50mM sample are listed in Figure 4 to reveal the final composition of the assembly when the all the assemblies had completed. The mutation into parallel structures obeys the docking/locking mechanism that the parallel fibril ends act as a template or molecular guidance for the incoming monomers.[12, 13] Therefore, both free monomers and free fibril ends are needed for the para-crystalline structures to propagate. Because peptides grown at increasing salt concentrations aggregated into larger particles, less free monomers and less free fibril ends were available in the solution. Once all available free peptides were used up, the structural mutations would stuck and not be able to proceed anymore. Therefore, as the salt concentration increased, the extent of the structural mutations was expected to decrease and the final assembly was expected to be more heterogeneous. Figure 4 indeed supported the heterogeneity hypothesis. In the 0 mM salt sample, the only para-crystalline structure present was the parallel fibers; for the 10 mM salt sample, the major assembly products were parallel fibers but some antiparallel structures also existed; the 25 mM salt sample comprised of antiparallel in-register, antiparallel/out-of-register, and parallel structures at nearly the same amounts, and finally, antiparallel structures dominated in the final assembly of the 50 mM salt sample.

The increase of the heterogeneity under high salt concentration was believed to result from the deficiency of free monomers and free fibril ends. To test if this is true, two future experiments are purposed here. Adding peptide monomers into the assembly should re-initiate the stuck mutation. In addition, sonicating the assembly could help break the particles and release free fibril ends. Similarly, the structural mutations should be able to continue to proceed into a higher extent, and the resulting final assembly should be less heterogeneous or even become homogenously parallel fibers.

2. E22Q Agitation Project

The IR spectra of the E22Q assembled under still, shaken, and stirred environments were illustrated in Figure 5 a-c, respectively. In all three graphs, the black dotted line was the spectrum of E22Q final assembly, which was known to compose of pure parallel fibers, obtained from Liang et al.'s study[7].

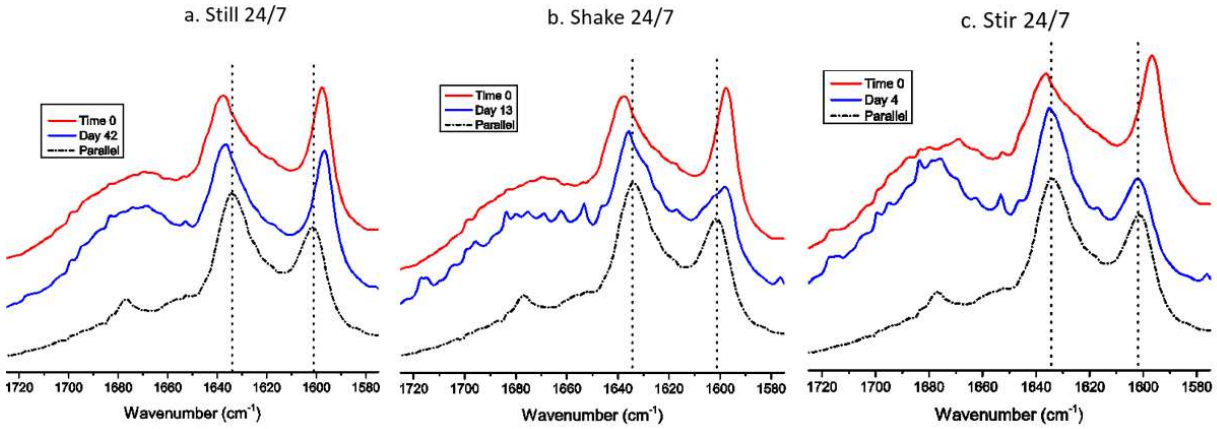

Figure 5. IR spectra of E22Q assembled at a). still environment (minimizing agitation); b). shaking environment (placing on a shaker); c). stirring environment (stirred by a stir bar). For each graph, the black dotted spectrum is the standard IR spectrum of parallel fibers.

Agitating by either shaking or stirring the sample during the assembly process provided shearing forces to the sample to against viscosity, helping to break the particles and the fibers to provide more fibril ends. Thus, the rate of assembly for both the shaken and the stirred samples should be higher relative to the still sample, in which agitation was kept at minimum. Figure 5 supported the hypothesis. For the still sample, the antiparallel to parallel mutation hadn't started in the first 42 days of the assembly, since the time 0 and day 42 spectra were similar to each other, and were different from the known parallel spectrum (Figure 5a). For the shaken sample, the ^{12}C and ^{13}C peaks moved toward each other and the intensity of the ^{13}C peak lowered from time 0 to day 13 (Figure 5b). However, since day 13 till day 42, the spectra no longer changed and were different from the known parallel spectrum (Figure 5b), implied that the mutation stuck in the middle for the shaken sample. For the stirred sample, the day 4 spectrum was similar to the known parallel spectrum (Figure 5c), indicated that the mutation finished at day 4, and the final assembly consisted of only parallel fibers. Therefore, the stirred sample had the fastest rate of assembly, followed by the shaken sample, and still E22Q assembled the slowest. Free fibril ends were indeed required for the propagation of para-crystalline structures. This project could thus serve as a supported experiment to the hypothesis purposed in the discussion of the first project.

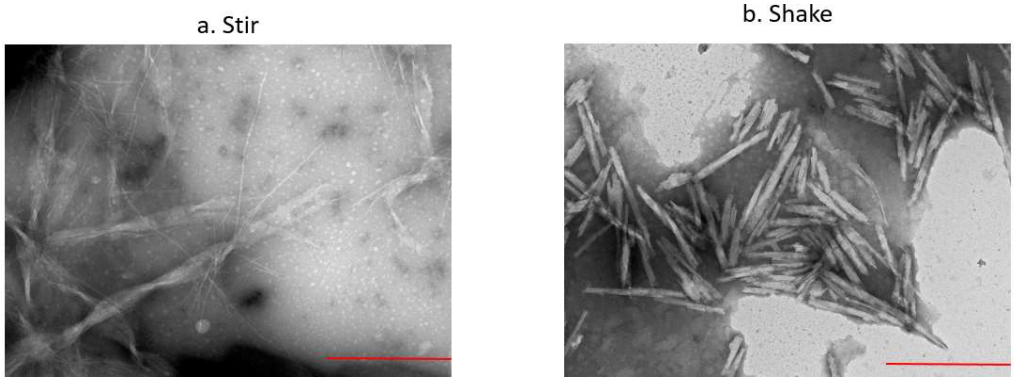

Figure 6. TEM images of E22Q at day 42 assembled in a). the stirring environment (assembly stirred by a stir bar), and b). the shaking environment (assembly placed on a shaker). Images are at the same scale, with the scale bars of both image being 500 nm.

The IR spectra indicated that the final assembly of the stirred sample composed only parallel fibers. Instead, the mutation was kinetically trapped at day 13, resulting in a mixture of antiparallel and parallel fibers in the final assembly of the shaken sample. TEM images revealed one possible reason for why this kinetic trap happened. TEM images of the shaken and the stirred E22Q assemblies at day 42, when structural mutations had either finished or trapped, were present in Figure 6a and Figure 6b. Individual twisted ribbons and long thin fibers could be seen in the final assembly of the stirred sample (Figure 6a). On the contrary, only short fibers were present in the shaken sample, and they were bundled together (Figure 6b). The bundling of the fibers might be due to the effect of shaking, since shaking drove solvent back and forth, and when the solvent was brought away from the structures, structures were easily to bundle with each other. Bundles were more stable structures than individual fibers[7], and they hindered the accessibilities of the fibril ends, explaining why the mutations stuck during the phase change of the shaken sample.

3. L17Q Project

3.1 Preliminary study revealed the ^{12}C-^{13}C peak coupling pattern of the L17Q IR spectra

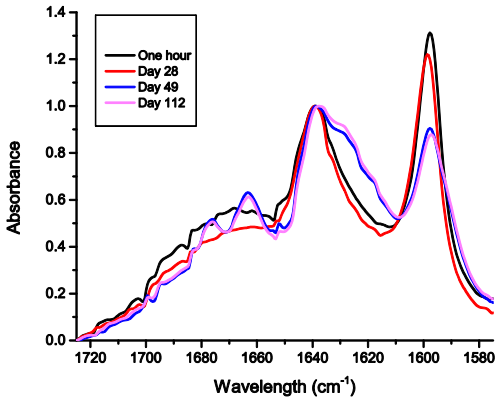

Figure 7. IR spectra of L17Q assembled in solvent of pH2.

A preliminary study was required in order to utilize the IE-IR technique to reveal the phase change during the assembly of the L17Q peptide. Because under acidic conditions, the glutamic acid at the C-terminus was deprotonated and not carrying its negative charge, L17Q in pH2 should be similar to E22Q, where the Q parallel code outweighed the electrostatic code and the parallel fibers completely replaced the antiparallel once. IR spectra of L17Q solvated in pH2 solvent were outlined in Figure 7. Structural mutation started at day 28 and stopped at day 49. During the mutation, no obvious change could be observed in the ^{12}C and ^{13}C peak positions, but the intensity of the ^{13}C peak decreased as the transition proceed (Figure 7).

3.2 Comparing L17Q assembly in pH2 vs pH7

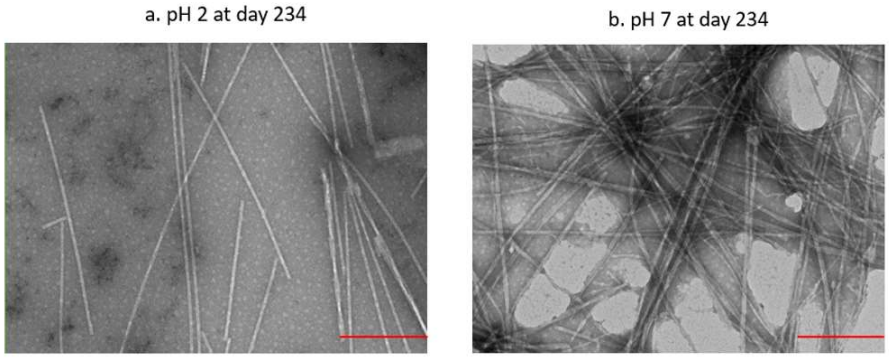

Figure 8. TEM images of L17Q assembled in solvent of a). pH2, and b). pH7 at day 234. Both images are adjusted to the same scale and the scale bar in each image represents 200 nm.

L17Q was dissolved in solvent of pH2 and pH7, respectively. The TEM images of the two samples at day 234 were shown in Figure 8. Under both pH conditions, peptides grew into homogeneous long, thin fibers, suggesting that L17Q in both the acidic and the neutral solvent propagated into the same final structures, most possibly parallel fibers. However, fibers were present individually in the pH2 solvent, whereas bundled in the pH7 solvent (Figure 8 a and b). The bundling of fibers in the pH7 solvent occurred due to salt bridges between the positively charge on the N-terminus lysine of one fiber and the negative charge on the C-terminus glutamic acid of the adjacent fiber. Based on the result of the E22Q agitation project, the bundling of the fibers in the pH7 condition indicated the possibility of kinetic traps during phase mutation from antiparallel to parallel structures because of the hindered access of free fibril ends.

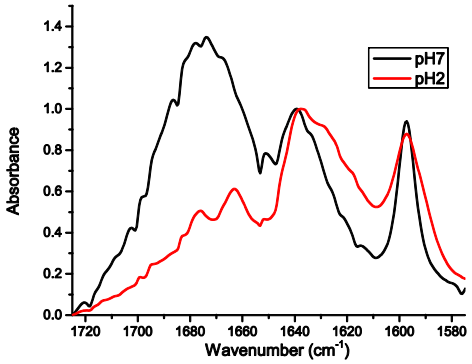

Figure 9. IR spectra of L17Q assembled in solvent of pH2 (red line) and pH7 (black line) at day 234.

Figure 9 includes two IR spectra, each belongs to the L17Q assembled in solvent of pH2 and pH7 at day 234. The intensity of the ^{13}C peak was about the same as that of the corresponding ^{12}C peak, and the two ^{13}C peak ended up at about the same height (Figure 9). It was thus able to conclude that the antiparallel to parallel phase change had occurred for the 17Q in either pH2 or pH7 solvent. Although L17Q in pH7 solvent possessed a strengthened electrostatic code, the Q parallel code was so strong to still be capable of driving the phase mutation to produce parallel fibers. This result reinforced the fact that in the full-length Aβ peptide a single substitution into Q leaded to Dutch syndrome.[8] In addition, the fact that most amyloid assemblies are thermodynamically more stable as parallel in-register arrays[14] suggested the possible relationships between this Q H-bonding association and the disease phase of most amyloids.

CONCLUSION

The Dutch mutant form of the nucleating core of the Aβ peptide of AD, Aβ(16-22) E22Q, aggregates into particles of larger size and at a greater rate in the presence of salt. With fewer free monomers at high salt concentrations, the mutation rate is slower and the intermediate assemblies appear to be kinetically trapped. The final assembly includes more heterogeneity with a mixture of antiparallel and parallel structures. This heterogeneity can be controlled by media dielectric which is important in our further consideration of the structures forming in the disease states.

This conclusion is reinforced by the stirring and shaking experiments. Shearing breaks the forming fibers to induce an increase in free fibril ends, and an increase in the rate of mutation from the antiparallel fibers to the thermodynamic parallel structures. Strikingly, without agitation this rate of transition was too slow to measure. This rate of mutation could be controlled by reducing either free peptide concentration or template ends.

Finally, substitutions within this peptide establish that the Q H-bonding cross-strand pair is stronger than the K/E electrostatic association, at least with L17Q. The impact of sequence dependence of the associations will need to be further explored, but clearly Q H-bonding is a very strong association and almost certainly play a role in disease causing amyloids as most of these assemblies are thermodynamically more stable as parallel in-register arrays. Whether these thermodynamic products are critical for disease etiology can now be further explored.

REFERENCE

1. Jucker, M.; Walker, L. C. Amyloid-β Pathology Induced in Humans. *Nature* **2013**, *501*, 45-51.
2. Dong, J.; Lu, K.; Lakdawala, A.; Mehta, A. K.; Lynn, D. G. Controlling Amyloid Growth in Multiple Dimensions. *Amyloid* **2006**, 13, 206-215.
3. Suh, Y. H. Amyloid Precursor Protein, Presenilins, and α-Synuclein: Molecular Pathogenesis and Pharmacological Applications in Alzheimer's Disease. *Pharmacological Reviews*. **2002**, *54*, 469–525.
4. Childers, W. S.; Anthony, N. R.; Mehta, A. K.; Berland, K. M.; Lynn, D. G. Phase Networks of Cross-β Peptide Assemblies. *Langmuir*, **2012**, 28, 6386-6395.
5. Lee, S.; Fernandez, E. J.; Good, T. A. Role Of Aggregation Conditions in Structure, Stability, and Toxicity of Intermediates in the Abeta Fibril Formation Pathway. Protein Science. **2007**, 16, 723–732.
6. Childers, W. S.; Mehta, A. K.; Bui, T. Q.; Liang, Y.; Lynn, D. G. Toward Intelligent Material. In *Molecular Self-Assembly - Advances and Applications*, 1st ed.; Pan Stanford Pub.: Singapore, **2012**, 1-36.
7. Liang, C.; Ni, R.; Smith, J. E.; Childers, W. S.; Mehta, A. K.; Lynn, D. G. Kinetic Intermediates in Amyloid Assembly. *J. Am. Chem. Soc.* **2014**, 136, 15146–15149.
8. Smith, J. E.; Liang, C.; Tseng, M.; Li, N.; Li, S.; Mowles, A. K.; Mehta, A. K.; Lynn, D. G. Defining the Dynamic Conformational Networks of Cross-β Peptide Assembly. *Isr. J. Chem.* **2015**, 763-769.
9. Šarić, A.; Chebaro, Y. C.; Knowles, T. P. J.; Frenkel, D. Crucial Role of Nonspecific Interactions in Amyloid Nucleation. *P. Natl. Acad. Sci. USA.* **2014**, 111, 17869–17874.
10. Anthony, N. R.; Mehta, A. K.; Lynn, D. G.; Berland, K. M. Mapping Amyloid-β(16-22) Nucleation Pathways Using Fluorescence Lifetime Imaging Microscopy. *Soft Matter* **2014**, 10, 4162–4172.
11. Hill, S. E.; Miti, T.; Richmond, T.; Muschol, M. Spatial Extent of Charge Repulsion Regulates Assembly Pathways for Lysozyme Amyloid Fibrils. *PLoS ONE*. **2011**, 6.
12. Esler, W. P.; Stimson, E. R.; Jennings, J. M.; Vinters, H. V.; Ghilardi, J. R.; Lee, J. P.; Mantyh, P. W.; Maggio, J. E. Alzheimer's Disease Amyloid Propagation By a Template-Dependent Dock-Lock Mechanism. *Biochemistry*. **2000**, 39, 6288–6295.
13. Nguyen, P. H.; Li, M. S.; Stock, G.; Straub, J. E.; Thirumalai, D. Monomer Adds to Preformed Structured Oligomers of Abeta-Peptides by a Two-Stage Dock-Lock Mechanism. *P. Natl. Acad. Sci. USA.* **2006**, 104, 111–116.
14. Peterson, S. A.; Klabunde, T.; Lashuel, H. A.; Purkey, H.; Sacchettini, J. C.; Kelly, J. W. Inhibiting Transthyretin Conformational Changes That Lead to Amyloid Fibril Formation. *PNAS.* **1998**, 95, 12956–12960.